IOP Publishing Journal of Physics D: Applied Physics
J. Phys. D: Appl. Phys. **40** (2007) 6969–6974 doi:10.1088/0022-3727/40/22/017

Electron-impact dissociation cross sections for CHF_3 and C_3F_8

J E Baio, H Yu, D W Flaherty, H F Winters and D B Graves

Department of Chemical Engineering, University of California, Berkeley, CA 94720, USA

Received 10 August 2007, in final form 5 October 2007
Published 2 November 2007
Online at stacks.iop.org/JPhysD/40/6969

Abstract
Absolute total dissociation cross sections, $\sigma_{t,diss}$, by electron-impact are reported for CHF_3 and C_3F_8 from 10 to 300 eV using the chemical gettering technique described by Winters and Inokuti (1982 *Phys. Rev.* A **25** 1420). Data are concentrated in the near-threshold region (10–30 eV). The thresholds for dissociation of CHF_3 and C_3F_8 are determined to be 10.4 eV and 11.9 eV, respectively. Ionization thresholds occur at 16 eV for CHF_3 and 16.2 eV for C_3F_8. Neutral dissociation cross sections of both CHF_3 and C_3F_8 are obtained by subtracting the ionization cross sections, $\sigma_{t,ion}$, from the total dissociation cross sections, $\sigma_{t,diss}$.

1. Introduction

The CHF_3 and C_3F_8 molecules are used in many of the plasma etching and cleaning processes employed in the semiconductor industry. Electron-impact dissociation of these inert feed gases produces chemically reactive species, including hydrogen and fluorine atoms and CF, CF_2 and CF_3 radicals. The dependability and accuracy of plasma chemistry models centres on the basic data describing electron–molecule interactions, specifically dissociation cross sections at electron energies near dissociation thresholds. Problems coupled with the discharge of stable greenhouse gases in the atmosphere have prompted studies of plasma dissociation and annihilation of perfluorocarbon (PFC) and hydrofluorocarbon (HFC) gases [1].

To properly model these processes, one must possess accurate values of electron-impact dissociation cross sections. However, only a small amount of electron-impact dissociation cross section data exists. Comprehensive surveys of electron interactions with CHF_3 and C_3F_8 (published by Christophorou *et al* and Christophorou and Olthoff) point out that the available measurements for total electron-impact dissociation cross sections, $\sigma_{t,diss}$, total ionization cross sections, $\sigma_{t,ion}$, and total neutral dissociation cross sections, $\sigma_{t,n}$, are few [2–5]. These surveys also reveal large discrepancies between the calculated and the measured total ionization cross sections [2–8]. In this paper, we present measurements of absolute total dissociation ($\sigma_{t,diss}$) and total ionization ($\sigma_{t,ion}$) cross sections for both CHF_3 and C_3F_8. In addition, we estimate values of $\sigma_{t,n}$ by subtracting $\sigma_{t,ion}$ from $\sigma_{t,diss}$, assuming the ionization processes are all dissociative [4, 9].

2. Measurements

Methods used to measure total dissociation cross sections are discussed in detail in earlier publications and will only be briefly outlined here [4, 10–14]. First, a monoenergetic beam of electrons, originating from a tungsten filament, travels through an experimental tube containing the parent gas (experimental pressure $\sim 5 \times 10^{-5}$ Torr). This beam of electrons is guided down the centre of the tube by a series of electrodes held at predetermined voltages, and a parallel magnetic field. In transit, the electrons dissociate and ionize gas molecules. If these fragments all adsorb on the walls, the total dissociation cross section is related to the total pressure change in the parent gas by way of the ideal gas law. Details of how the total dissociation cross sections are related to total pressure change can be found in appendix A. One complication of this method is the contribution of the molecular fragmentation by the electron-generating filament, as noted below and in appendix A.

Results from a typical experimental run, a plot of the logarithm pressure versus time, can be found in figure 1. Constants $C_{Filament}$ and C_{F+E} are defined in appendix A, and are equal to the slopes of the different linear segments found in figure 1. All slopes are derived using least-squares fits with a correlation of at least $R^2 = 0.99$. This procedure of measuring the experimental constants $C_{Filament}$ and C_{F+E} is identical to that used in previous investigations [4, 14]. These constants represent the two phases of the experimental run: (1) where fragmentation is induced only by the filament and (2) where dissociation is induced by both the beam of electrons and the filament.

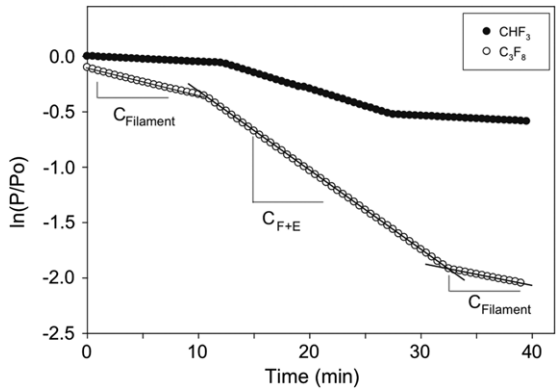

Figure 1. Example of typical raw data from this investigation. CHF_3 and C_3F_8 at $E = 100$ eV, $P_o = 5 \times 10^{-5}$ Torr.

In order to successfully apply the ideal gas law, as it equates the number of molecular fragmentation events to the pressure change, the parent gas must satisfy three criteria established by Winters and Inokuti [4]. First, undissociated ions and undissociated excited neutrals cannot leave the gas phase as a result of surface reactions. Secondly, all dissociation products must irreversibly adsorb to the walls of the working volume or getter. Finally, fragments must not recombine on surfaces within the system to reform the parent gas. Since Winters and Inokuti showed that both CHF_3 and C_3F_8 meet these three essential criteria, the measurements reported here yield total dissociation cross sections [4]. Desorption of impurities, such as CO and CO_2, from within this system can affect the pressure measurements during the experiment. Therefore, an impurity getter is created within the apparatus by evaporating a small amount of titanium before each test, creating a film that will adsorb the impurity gas without reacting with the parent gas.

Excitation and dissociation can be measured in several different ways. However, most require absolute measurements of gas density. In this investigation, cross sections are determined from the slope of the pressure versus time curve. This is inherently easier than accurately measuring the absolute pressure. The number of molecules leaving the gas phase is accurately resolved by the change in pressure, thereby eliminating the chance of double counting ion-induced secondary electrons or doubly charged ions.

3. Apparatus

Experiments are conducted in a closed volume containing the experimental tube, a MKS spinning rotor gauge and a newly evaporated titanium getter. Components of this working volume are linked to a larger volume by way of an ultra-high vacuum valve, containing an Inficon mass spectrometer.

The experimental tube is identical to the tube used by Winters and Inokuti and Flaherty *et al* in past investigations [4, 14]. At the top of the tube is a 0.254 mm tungsten filament, F_W. This resistively heated filament emits electrons that travel down the tube and are collected at the electron sink, or target, located at the opposite end (figure 2). These electrons are maintained as a beam by a solenoid generated, 300 G magnetic field parallel to the electron beam. The electron energy is

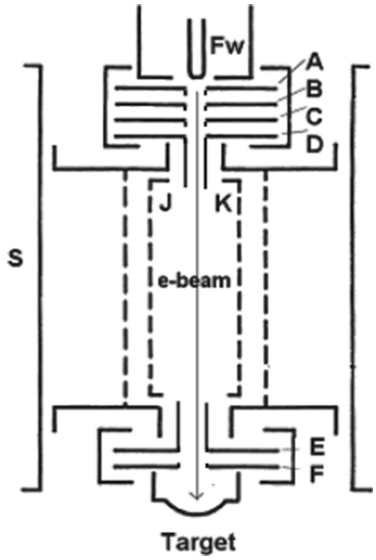

Figure 2. Schematic of experimental tube: F_W is the tungsten filament, A–F are the control electrodes that run down the inside of the tube, J and K are a set of two symmetric semicircular tungsten grids and S is the solenoid surrounding the tube.

determined by the potential difference between the filament and a virtually field free region maintained in the central volume of the tube. This region is defined by electrodes D, F and two semicircular tungsten grids, J and K (figure 2). Electrons are drawn from the filament by the potentials applied to electrodes A, B and C. During all experiments, electrodes A, B and C were held at approximately 7, 6 and 3 V, respectively. As electrons travel through electrodes A, B and C, the electron energy is kept below the dissociation threshold. Electrodes D, F and grids, J and K, are biased to produce the desired experimental energy. Spot welded on electrodes D and E are small cylinders (diameter ~0.42 mm) that point towards the centre of the tube, minimizing the current to electrodes D, E and F, and maximizing the current to the target. Hence, the effective dissociation path length for these electrons is the distance between electrodes D and F.

The effective ionization path length is equal to the distance between the two ends of the cylinders. A small electric field perpendicular to the electron beam is created by placing potentials of +2 V and −2 V on a set of two symmetric semicircular tungsten grids, J and K. This allows ions to be extracted without altering the energy of the electron beam.

To prevent dissociation by secondary electrons originating from the target, a 300 V bias is placed between F and the target. As mentioned in Flaherty *et al*, this bias produces some dissociation; however, since these events occur in both of the operating regimes, they are subtracted out with the reactions at the filament [14].

It was also shown by Winters and Inokuti that cross section values are independent of variations in operating conditions, such as total pressure of the apparatus, electron beam current, draw out field and magnetic field [4].

4. Energy calibration

Due to the existence of a small voltage drop across the filament, the electron beam energy varied slightly, creating

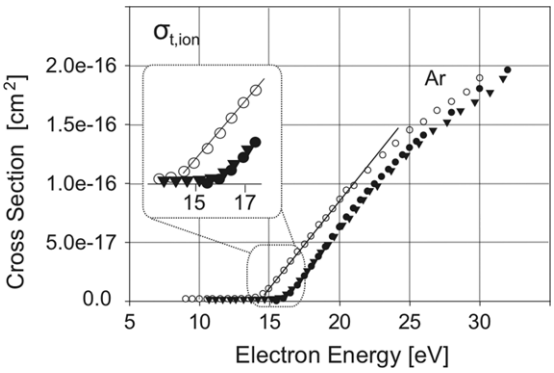

Figure 3. A comparison of measured total ionization cross sections, $\sigma_{t,ion}$, for Ar used in our energy calibration. (●) are values taken from Rapp and Englander-Golden, (○) are the authors' measurements, and (▼) are measurements normalized to values taken from Rapp and Englander-Golden [15]. The solid line illustrates how the data was extrapolated to find the threshold of dissociation.

some uncertainty in the absolute energy of the beam. In order to calibrate the electron energy, total ionization cross sections for argon were measured from 13 to 300 eV and then compared with values published by Rapp and Englander-Golden [15]. This calibration process involved determining the ionization threshold by extrapolating a linear fit of the near-threshold data and, then, adjusting the energy scale of the present measurements to agree with Rapp and Englander-Golden's ionization threshold value. For all experiments, the difference between these two values was used to correct the energy scale. Figure 3 illustrates the agreement between these calibration measurements and Rapp and Englander-Golden [15]. At one point during a series of C_3F_8 experiments, the filament had to be replaced which made it necessary to recalibrate the energy scale for the later set of data. In addition, the differences in magnitude between our measured total ionization cross sections for argon, and those reported by Rapp and Englander-Golden provided the ion collection efficiency of the system (67%).

5. Error

The sources of experimental error included the inability to track individual electrons from the filament to the target which created uncertainty in the exact path length of the electron beam (±9%), errors in the measurement of the experimental volume (±2%) and errors in the measurement of the electron beam current (±3%). Combined these errors lead to an estimate of ±11% for the overall error in the measured cross section values [16].

6. Results

Total dissociation cross sections, $\sigma_{t,diss}$, for CHF_3 and C_3F_8 were measured for electron energies ranging from 10 to 300 eV (figure 4 and tables 1 and 2). Extrapolations of the near-threshold values, of total dissociation cross sections (figures 5 and 6), yielded dissociation thresholds for both CHF_3 and C_3F_8 of 10.4 eV and 11.9 eV, respectively. As figure 4 illustrates, the measured total dissociation cross section values are smaller than those reported earlier by Winters and Inokuti [4].

Table 1. Values of total dissociation cross sections ($\sigma_{t,diss}$), total ionization cross sections ($\sigma_{t,ion}$) and total neutral cross sections ($\sigma_{t,n}$) for CHF_3. Cross section values are in units of 10^{-16} cm^2.

Electron energy (eV)	$\sigma_{t,diss}$	$\sigma_{t,ion}$	$\sigma_{t,n}$
10	—	—	—
11	0.20	—	—
12	0.23	0.04	0.16
13	0.32	0.04	0.28
14	0.38	0.04	0.34
15	0.64	0.04	0.56
16	0.58	0.06	0.59
17	0.83	0.12	0.71
18	1.03	0.20	0.84
19	1.12	0.35	0.77
20	1.27	0.51	0.75
21	1.37	0.64	0.72
22	1.42	0.83	0.59
23	1.61	0.98	0.63
24	1.72	1.12	0.58
25	1.76	1.25	0.56
26	1.96	1.40	0.58
27	2.15	1.56	0.57
28	2.19	1.72	0.48
29	2.43	1.87	0.56
30	2.68	1.98	0.68
40	3.80	3.00	0.80
50	4.29	3.75	0.54
75	5.10	4.78	0.32
100	5.12	5.21	—
125	5.28	5.35	—
200	4.93	5.20	—
300	4.41	—	—

It is believed that these dissimilarities arose due to the varied strengths of the bias that suppressed secondary electrons originating from the target. Winters and Inokuti used a 75 V bias between F and the target, while in the investigation presented here, a 300 V bias was employed [4]. Variations between $\sigma_{t,diss}$ values presented here and those reported by Winters and Inokuti, except for a single data point at 22 eV, are within the experimental error for this experiment (11%). We believe the larger bias did a better job of suppressing secondary electrons. Therefore, we suggest that the total dissociation cross section measurements presented here are more accurate than the previously presented measurements.

Values of $\sigma_{t,ion}$, for CHF_3 and C_3F_8, are found in figure 7. As mentioned before the system cannot collect 100% of the ions produced. Therefore, it is necessary to normalize the total ionization cross section values. However, instead of normalizing our measurements of total ionization cross sections to previously measured or calculated values, the approach used by Flaherty *et al* we normalized the peak total ionization cross section to the peak value of the total dissociation cross sections [14]. The lack of a parent peak in the mass spectra indicates that all electronic excitations of CHF_3 and C_3F_8 lead to dissociation by ionization [9]. Therefore, at high electron energies total ionization cross sections should never exceed the total dissociation cross sections. Consequently, the values presented here are the maximum allowed total ionization cross sections. This normalization

Table 2. Values of total dissociation cross sections ($\sigma_{t,diss}$), total ionization cross sections ($\sigma_{t,ion}$) and total neutral cross sections ($\sigma_{t,n}$) for C_3F_8. Cross section values are in units of 10^{-16} cm^2.

Electron energy (eV)	$\sigma_{t,diss}$	$\sigma_{t,ion}$	$\sigma_{t,n}$
10	0.05	—	—
11	0.17	0.11	0.05
12	0.24	0.12	0.08
13	0.29	0.13	0.22
14	0.78	0.13	0.13
15	0.75	0.14	0.58
16	1.25	0.18	0.99
17	1.06	0.29	0.66
18	1.72	0.46	1.00
19	2.06	0.67	1.37
20	2.03	1.00	0.85
21	2.67	1.10	1.30
22	3.12	1.41	1.25
23	2.60	1.79	1.12
24	3.09	2.06	0.81
25	3.88	2.31	0.93
26	3.71	2.68	1.12
27	4.18	2.92	1.20
28	4.26	3.29	0.98
29	4.77	3.55	1.21
30	5.09	3.74	1.39
40	6.93	5.77	1.16
50	8.12	7.17	0.95
75	9.41	9.09	0.32
100	9.95	9.91	—
125	10.4	10.3	—
200	9.37	9.48	—
250	9.30	9.32	—
300	8.43	—	—

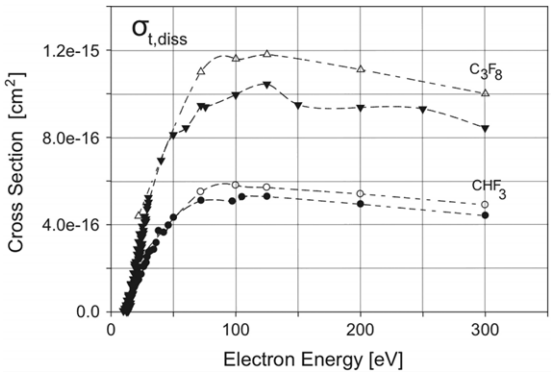

Figure 4. Total dissociation cross sections, $\sigma_{t,diss}$, for both CHF_3 (●,○) and C_3F_8, (▼,▽). Solid symbols are values presented here while the open symbols are taken from Winters and Inokuti [4].

implies that the system's ion collection efficiencies are 45% for $CHF_3$and 56% for C_3F_8.

Plotted in figure 7 are previous measurements of $\sigma_{t,ion}$ for CHF_3 by Iga *et al* and Onthong *et al* A reactive flow technique was employed by Iga *et al*, while Onthong *et al* calculated $\sigma_{t,ion}$ by the Duetsch–Mark formalization [6, 8]. As figure 7 points out, the maximum $\sigma_{t,ion}$ data set presented here has a slightly larger peak but as a whole generally falls within 18% of the peak values by Iga *et al* and 22% of the peak values of Onthong *et al* [6, 8]. By extrapolating the near-threshold total ionization cross sections, the threshold of ionization for CHF_3 was determined to be 16 eV (figure 5).

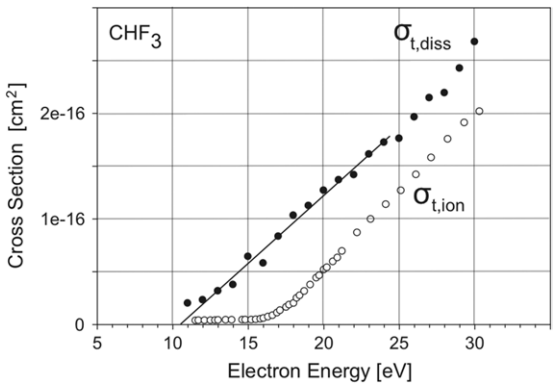

Figure 5. Values of near-threshold (10–30 eV) total dissociation cross sections, $\sigma_{t,diss}$ (●) and total ionization (assumed dissociative) cross sections, $\sigma_{t,ion}$ (○), for CHF_3. The solid line illustrates how the data was extrapolated to find the threshold of dissociation.

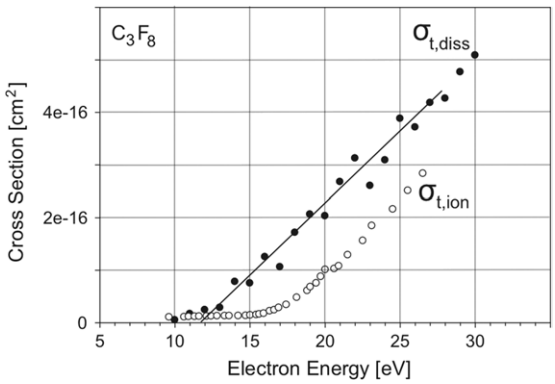

Figure 6. Values of near-threshold (10–30 eV) total dissociation cross sections, $\sigma_{t,diss}$ (●) and total ionization (assumed dissociative) cross sections, $\sigma_{t,ion}$ (○), for C_3F_8. The solid line illustrates how the data was extrapolated to find the threshold of dissociation.

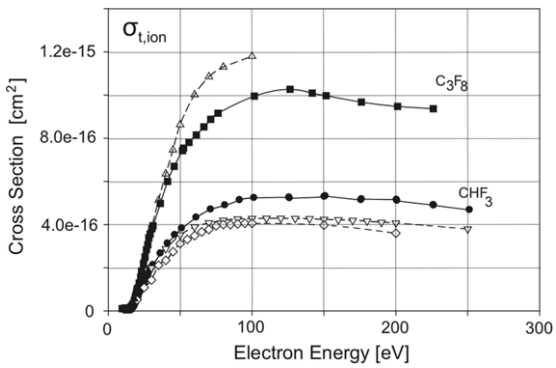

Figure 7. Plots of total ionization (assumed dissociative) cross sections, $\sigma_{t,ion}$, for CHF_3 and C_3F_8: solid symbols (present data); (◊) and (▽) are values of $\sigma_{t,ion}$ for CHF_3 taken from Iga *et al* [6] and Onthong *et al* [8], respectively; (△) are values of $\sigma_{t,ion}$ for C_3F_8 taken from Christophorou and Olthoff [5].

In their review of current electron-impact cross section data for C_3F_8, Christophorou and Olthoff recommend a set of total ionization cross sections values. This set was made up of an average of the measurements by Poll and Meichsner and of Nishimura *et al* (figure 7) [5,17,18]. The total ionization cross sections presented by Christophorou and Olthoff are larger than the maximum allowed total ionization values

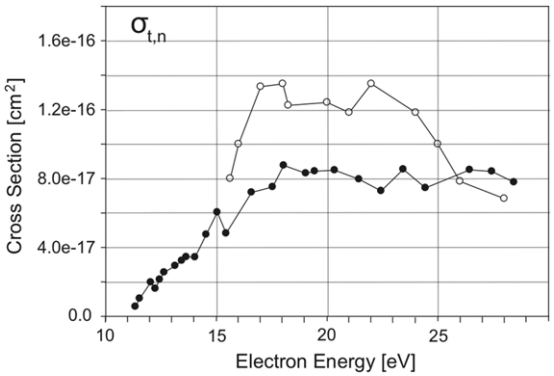

Figure 8. Total neutral dissociation cross sections, $\sigma_{t,n}$, for CHF_3. (●) are values presented here and (○) are taken from Morgan *et al* [19].

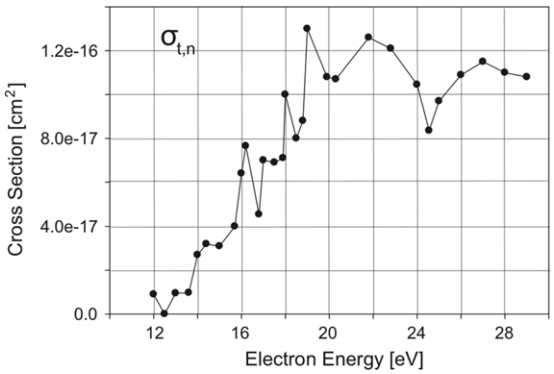

Figure 9. Total neutral dissociation cross sections, $\sigma_{t,n}$, for C_3F_8.

presented here. In fact, it should be noted that the average total ionization data set recommended by Christophorou and Olthoff has a peak 17% higher than the peak of our measured total dissociation cross sections. One point of agreement was that the C_3F_8 total ionization data recommended by Christophorou and Olthoff was extrapolated to yield a threshold of ionization at 15.5 eV. A similar extrapolation of the ionization cross sections measured here yielded a threshold of ionization at 16.2 eV (figure 6).

The minimum total neutral dissociation cross sections, $\sigma_{t,n}$, for CHF_3 and C_3F_8 can be found in figures 8 and 9, respectively. These values are calculated by subtracting the maximum values of $\sigma_{t,ion}$ from the measured values of $\sigma_{t,diss}$. Also present in figure 8, are values of $\sigma_{t,n}$ for CHF_3 previously calculated and published by Morgan *et al* [19]. Despite the differences between these two data sets, the peak clearly occurs at 18 eV. In the case of C_3F_8 a peak value of 1.3×10^{-16} cm^2 occurs at 19 eV. To the authors' knowledge, there are no other published direct measurements of total neutral dissociation cross sections for C_3F_8 [5].

7. Concluding remarks

In summary, total dissociation thresholds for CHF_3 and C_3F_8 occurred at 10.4 eV and 11.9 eV, respectively. Ionization thresholds occurred at 16 eV for CHF_3 and 16.2 eV for C_3F_8. The present measurements of $\sigma_{t,diss}$, for both CHF_3 and C_3F_8, are smaller than previously published values [4]. The data presented here for CHF_3 and C_3F_8, and previous measurements of C_2F_6 by Flaherty *et al*, revealed total dissociation cross section measurements that were ∼10% lower than those previously measured by Winters [14]. It is believed that these small discrepancies arose from the present method of effectively suppressing secondary electrons. Therefore, we recommend slightly reducing, total dissociation cross section values for N_2 and CH_4, previously published by Winters by ∼10% [10–13].

The measured maximum CHF_3 total ionization cross sections, $\sigma_{t,ion}$, are slightly larger than the values recently measured by Iga *et al* and Onthong *et al* [6, 8]. The total ionization cross sections presented here for C_3F_8 are substantially smaller than those recommended by Christophorou and Olthoff [3].

Acknowledgments

The authors acknowledge IBM Almaden Research Center for donating much of the experimental apparatus. This research was funded in part by the NSF-SRC ERC for Environmentally Benign Semiconductor Manufacturing. JEB would also like to thank A.Branham and the Patek Lab for all of their input.

Appendix A

The total dissociation cross section is related to the total pressure change in the parent gas by way of the ideal gas law:

$$\frac{dN(t)}{dt} = \left[\frac{V}{kT}\right]\frac{dP(t)}{dt}, \tag{A.1}$$

where $P(t)$ is the pressure, T is the temperature and $N(t)$ is the number of gas phase molecules in the closed working volume, V. For many gases, fragmentation events can be credited to either the electron–molecule collisions or to interactions with the tungsten filament:

$$\frac{dN_{Total}}{dt} = \frac{dN_{Filament}}{dt} + \frac{dN_{Emission}}{dt}. \tag{A.2}$$

During the experiment, the temperature of the filament is held constant. Thus, the dissociation taking place at the filament is only a function of N and can be reduced to

$$\frac{dN_{Filament}}{dt} = -C_{Filament} \cdot N, \tag{A.3}$$

where $C_{Filament}$ is an experimentally determined constant. Similarly, the dissociation rate due to the electron–molecule collisions can be described by

$$\frac{dN_{Emission}}{dt} = -\frac{N_e D \sigma_{t,diss} N}{V}, \tag{A.4}$$

where N_e is the number of electrons per second that travel a path length, D, down the tube and $\sigma_{t,diss}$is the total dissociation cross section. The overall rate of fragmentation can be expressed as

$$\frac{dN_{Total}}{dt} = \frac{dN_{Filament}}{dt} + \frac{dN_{Emission}}{dt} = -C_{F+E} \cdot N$$
$$= -\left(C_{Filament} + \frac{N_e D \sigma_{t,diss}}{V}\right) \cdot N. \tag{A.5}$$

Solving for $\sigma_{t,diss}$yields

$$\sigma_{t,diss} = \frac{V}{N_e D}\left(C_{F+E} - C_{Filament}\right). \tag{A.6}$$

References

[1] Tonnisd E J, Gravesd D B, Vartanian V H, Beu L, Lii T and Jewett R 2000 *J. Vac. Sci. Technol.* A **18** 393
[2] Christophoroud L G, Olthoff J K and Rao M V V S 1997 *J. Phys. Chem. Ref. Data* **26** 1
[3] Christophorou L G and Olthoff J K 1999 *J. Phys. Chem. Ref. Data* **28** 967
[4] Winters H F and Inokuti M 1982 *Phys. Rev.* A **25** 1420
[5] Christophorou L G and Olthoff J K 1998 *J. Phys. Chem. Ref. Data* **27** 889
[6] Iga I, Sanches I P, Srivastava S K and Mangan M 2001 *Int. J. Mass Spectrom.* **208** 159
[7] Beran J A and Kevan L 1969 *J. Phys. Chem.* **73** 3866
[8] Onthong U, Duetsch H, Becker K, Matt S, Probst M and Mark T D 2002 *Int. J. Mass Spectrom.* **214** 53
[9] Majer J R 1961 *Adv. Fluorine Chemistry* ed M Stacy *et al* (London: Butterworths) **2** p 55
[10] Winters H F 1966 *J. Chem. Phys.* **44** 1472
[11] Winters H F, Horne D E and Donaldson E E 1964 *J. Chem. Phys.* **41** 2766
[12] Winters H F 1975 *J. Chem. Phys.* **63** 3462
[13] Winters H F 1979 *Chem. Phys.* **36** 353
[14] Flaherty D W, Kasper M A, Baio J E, Graves D B, Winters H F, Winstead C and McKoy V 2006 *J. Phys. D: Appl. Phys.* **39** 4393
[15] Rapp D and Englander-Golden P 1965 *J. Chem. Phys.* **43** 1464
[16] Taylor J R 1997 *An Introduction to Error Analysis: The Study of Uncertainties in Physical Measurements* (Sausalito, CA: University Science Books) p 56
[17] Polld H U and Meichsner J 1987 *Contrib. Plasma Phys.* **27** 359
[18] Nishimura H, Huod W M, Alid M A and Kimd Y K 1999 *J. Chem. Phys.* **110** 3811
[19] Morgan W L, Winstead C and McKoy V 2001 *J. Appl. Phys.* **90** 4